JOURNAL OF GEOPHYSICAL RESEARCH: OCEANS, VOL. 118, 2507–2519, doi:10.1002/jgrc.20185, 2013

Dense water formation around islands

Michael A. Spall[1]

Received 31 December 2012; revised 28 March 2013; accepted 29 March 2013; published 17 May 2013.

[1] Basic constraints on the dense water formation rate and circulation resulting from cooling around an island are discussed. The domain under consideration consists of an island surrounded by a shelf, a continental slope, and a stratified ocean. Atmospheric cooling over the shelf forms a dense water that penetrates down the sloping bottom into the stratified basin. Strong azimuthal flows are generated over the sloping bottom as a result of thermal wind. Thermally direct and indirect mean overturning cells are also forced over the slope as a result of bands of convergent and divergent Reynolds stresses associated with the jets. The Coriolis force associated with the net mass flux into the downwelling region over the slope is balanced by these nonlinear terms, giving rise to a fundamentally different momentum budget than arises in semienclosed marginal seas subject to cooling. A similar momentum balance is found for cases with canyons and ridges around the island provided that the terms are considered in a coordinate system that follows the topography. Both eddy fluxes and the mean overturning cells are important for the radial heat flux, although the eddy fluxes typically dominate. The properties of the dense water formed over the shelf (temperature, diapycnal mass flux) are predicted well by application of baroclinic instability theory and simple heat and mass budgets. It is shown that each of these quantities depends only on a nondimensional number derived from environmental parameters such as the shelf depth, Coriolis parameter, offshore temperature field, and atmospheric forcing.

Citation: Spall, M. A. (2013), Dense water formation around islands, *J. Geophys. Res. Oceans*, *118*, 2507–2519, doi:10.1002/jgrc.20185.

1. Introduction

[2] Dense waters are formed in many regions of the global ocean, including the interior of semienclosed marginal seas, and on shallow shelves both along continental boundaries and around islands. Recent theoretical, numerical, and observational studies have related the properties of waters formed in marginal seas to a balance between atmospheric forcing and lateral advection by mesoscale eddies [*Visbeck et al*., 1996; *Marshall and Schott*, 1999; *Spall*, 2004, 2011, 2012; *Straneo*, 2006; *Isachsen and Nost*, 2012]. Cyclonic boundary currents are a key player in the buoyancy budgets by transporting light water from outside the marginal sea, providing a buoyancy source for mesoscale eddies to balance atmospheric forcing, and by transporting modified waters out of the marginal sea. Much of the dynamics and thermodynamics inherent in closing the basin-scale budgets of heat, fresh water, and mass rely on along-boundary changes in the cyclonic boundary current [*Spall*, 2011, 2012]. The net downwelling within the buoyancy-forced marginal sea takes place near the boundary and is supported by the along-boundary pressure gradient, even though the majority of the buoyancy forcing may be located in the basin interior [*Spall*, 2010].

[3] There have been numerous studies of dense water formation over a shelf. Some consider only localized forcing, as might result from coastal polynyas in the Arctic Ocean [*Gawarkiewicz and Chapman*, 1995; *Chapman and Gawarkiewicz*, 1997]. Others consider periodic channels with a sloping bottom along one side forced by surface cooling [*Kikuchi and Wakatsuchi*, 1999; *Pringle*, 2001] or a specified inflow of dense water over the shelf [*Jiang and Garwood*, 1996]. In each case, it has been found that lateral eddy fluxes are important for the spread of dense water away from the formation regions and across the sloping bottom. Less attention has been paid to momentum budgets and, in particular, how water is supplied to regions of downwelling.

[4] There have also been numerous studies of dense water formation near islands such as Iceland, St. Lawrence Island, and Antarctica [e.g., *Danielson et al*., 2006; *Foldvik et al*., 2004; *Pickart et al*., 2010; *Stewart and Thompson*, 2012]. However, each region differs in many details, (topography, forcing, presence of ice, large-scale circulation, thermobaricity) so that a universal theory that applies to all of these regions has proved difficult to develop. However, there are some general aspects of the problem of dense water formation around an island that warrant focussed study. In particular, a key feature of this problem that distinguishes it from convection within a marginal sea is that the island's topography and coastline are periodic in the

[1]Department of Physical Oceanography, Woods Hole Oceanographic Institution, Woods Hole, Massachusetts, USA.

Corresponding author: M. Spall, Department of Physical Oceanography, Woods Hole Oceanographic Institution, Woods Hole, MA 02543, USA. (mspall@whoi.edu)

2169-9275/13/10.1002/jgrc.20185

azimuthal direction. This requires that the pressure gradient term integrate to zero around the island. Since it is the pressure gradient term that controls the net downwelling in semienclosed marginal seas, it is anticipated that downwelling around islands must be maintained in a fundamentally different way than downwelling in marginal seas. A primary question is, if there is to be Eulerian downwelling associated with an export of dense water from the shelf to the deep basin interior, how is this mass budget closed? As will be shown, this is quite different from the mass budget in density space, or simply asking how the export of dense water is balanced by the import of light water. The main purpose of this study is to explore the consequences of this periodic condition on the processes of water mass transformation and downwelling around an island subject to buoyancy loss. Note that a similar constraint should be applicable to water mass transformation on shelves in enclosed basins. The underlying dynamics of such periodic flows are most readily revealed using idealized configurations of islands with a shelf and continental slope and, in some cases, canyons and ridges.

2. Circulation Forced by Cooling Over a Shelf

[5] The basic problem of dense water formation around an island is first considered using an eddy-resolving configuration of the Massachusetts Institute of Technology primitive equation general circulation model [*Marshall et al*., 1997] The circulation forced by cooling around an island will be introduced by a configuration with an island of 150 km radius within a stratified ocean basin (Figure 1). The shelf region around the island is 75 km wide and 100 m deep and flat. The surrounding ocean is 680 m deep and the transition between the shelf and deep ocean is achieved by a linearly sloping bottom with slope 0.003. This gives a width of the continental slope of 193 km. The sensitivity to these parameters will be explored in the following section. The initial stratification is $N^2 = (g/\rho_0)/\partial\rho/\partial z = 1.25 \times 10^{-5}\mathrm{s}^{-2}$, which gives a baroclinic deformation radius of 25 km in the open ocean. The model horizontal resolution varies from 3 km for $|x,y| < 387$ km, 6 km for 387 km $< |x,y| < 489$ km, and 12 km for 489 km $< |x,y| < 700$ km, where x and y are measured from the center of the domain (Figure 1). There are 30 levels in the vertical, ranging from 10 m in the upper 100 m to 50 m over the deepest 250 m. While the island is small compared to a typical ocean basin, the perimeter of the island is large compared to the baroclinic deformation radius and the natural spatial scales of the mean and time-dependent currents.

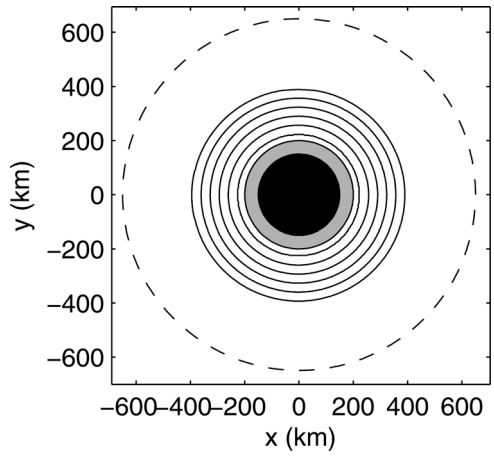

Figure 1. Bottom topography and model domain. Cooling is over the shelf (light gray area) and full depth restoring is at radius greater than 650 km (dashed line). The island is shaded black.

[6] The model is forced by restoring the sea surface temperature toward 0°C with time scale $\tau = 10$ days over the shelf (radius less than $R_c = 200$ km). This is equivalent to a restoring strength of $47.5\mathrm{Wm}^{-2}\mathrm{C}^{-1}$. There is no surface buoyancy forcing offshore of 200 km radius. Calculations have been carried out with buoyancy forcing over the whole domain but they do not change any of the main results below. Also, isolating the forcing to the shelf helps to identify the source regions for the waters that are transported onto the shelf. This localized forcing differs from the uniformly cooled laboratory experiments with sloping topography by *Condie and Rhines* [1994]. The stratification is restored toward the initial stratification at radius greater than 650 km with a time scale of 10 days. This ultimately provides a source of heat to balance the cooling around the island and allows for equilibrium solutions to be obtained. There is no forcing of momentum at the surface. *Stewart and Thompson* [2012] considered a similar configuration in a periodic channel but with a surface wind stress, which they found to be very important for the export of dense water formed on the shelf.

[7] Details of the model configuration and subgridscale parameterizations can be found in Appendix A.

[8] The model is initialized at rest and run for a period of 10 years to statistically equilibrated solutions, as indicated by time series of water mass properties and basin-averaged kinetic and potential energy. The model is then run for an additional 200 days with output saved every 5 days, during which time the analysis is carried out.

2.1. Eulerian Mean Fields

[9] Sections of the mean temperature, azimuthal velocity, radial velocity, and vertical velocity are shown in Figure 2. Each of these quantities was averaged in the azimuthal direction. The temperature shows the presence of cold water over the shelf, which penetrates down the sloping bottom in a relatively thin layer. The warmer waters provided by the offshore stratification are lifted upward over the continental slope such that the isotherms are nearly parallel to the bottom. This strong baroclinic shear is largely stabilized by the steep bottom slope, as expected from linear theory [*Blumsack and Gierasch*, 1972]. The isotherms outcrop over the sloping topography near the shelf break.

[10] The horizontal density gradient that arises as a result of the sloping isopycnals gives rise to a strong baroclinic current in the azimuthal direction (Figure 2b). The surface velocity is $O(20\,\mathrm{cm\,s}^{-1})$ in the direction such that shallow water is on the left, cyclonic in this northern hemisphere calculation. This is opposite to the direction of topographic wave propagation. However, near the bottom, the azimuthal velocity changes direction over the slope so that it is in the direction of wave propagation, albeit at much slower speeds than the surface velocity. There is also a

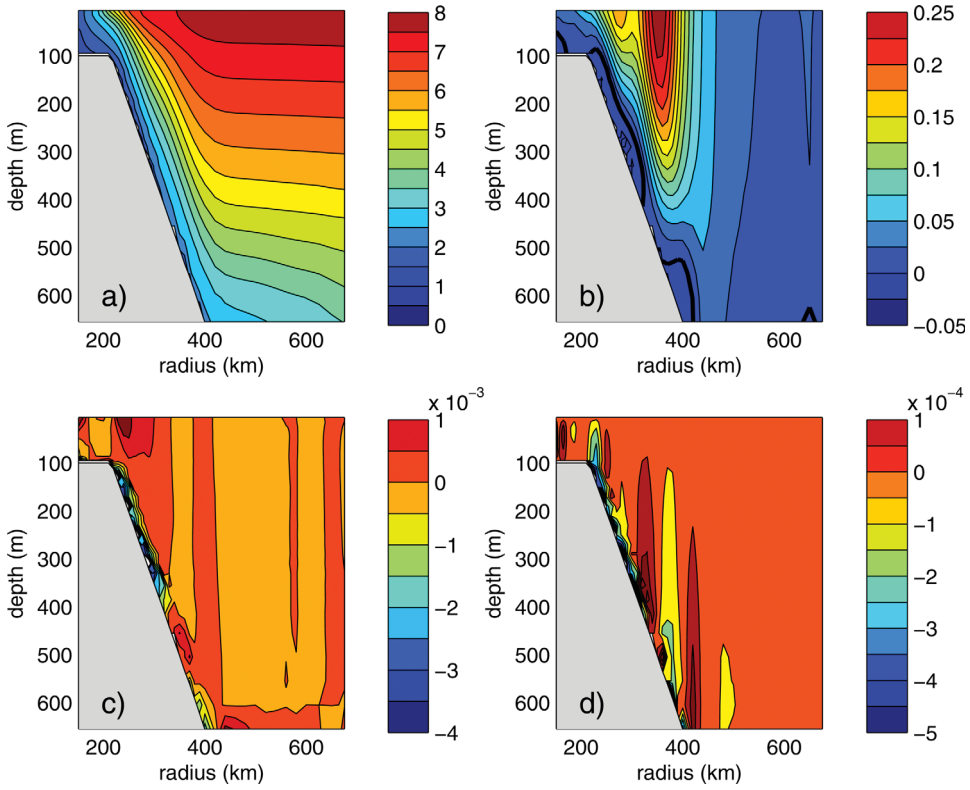

Figure 2. Mean sections of (a) temperature (°C); (b) azimuthal velocity, positive into the page (m s^{-1}); (c) radial velocity, positive toward the island (m s^{-1}); and (d) vertical velocity (m s^{-1}).

suggestion of multiple local maxima in the surface velocity, as will be discussed further below.

[11] The azimuthal velocity at the sloping bottom drives a downslope flow of $O(0.5\,\mathrm{cm\,s^{-1}})$ in the bottom Ekman layer between 200 and 320 km radius (Figure 2c). The along-slope bottom velocity is $O(2\ \mathrm{cm\,s^{-1}})$, giving a downslope angle in the bottom boundary layer of approximately 15°. In order to conserve mass over the sloping region, there is onshore flow that is strongest at the surface but onshore at all depths above the bottom boundary layer. The mean onshore/offshore flow at the shelf break is very small. There are two regions of onshore flow at the bottom, one over the outer slope and one over the flat interior. The flow above these onshore flows is offshore, as required to balance mass.

[12] The mean radial velocity must be ageostrophic because the pressure term exactly drops out when integrated along a closed contour. One can infer from the radial velocity that there are regions of mass convergence and divergence at the transition from offshore to onshore flow in the bottom boundary layer. This drives alternating regions of upwelling and downwelling over the slope (Figure 2d). There is a region of downwelling at the shelf break and upwelling over the outer slope. There is a second region of downwelling near the outer limit of the topography and upwelling at the edge of the offshore barotropic flow.

[13] This pattern of alternating upwelling and downwelling regions extends across the region of sloping topography. Wider sloping regions (weaker bottom slopes) result in more regions of convergence and divergence. Examples of the azimuthal velocity for several different bottom slopes are shown in Figure 3. For the narrowest topography, there is only one region of negative azimuthal flow near the bottom. For the central case in Figure 2b, there are two regions of negative flow. As the region of the sloping bottom gets wider, the number of counterflowing regions increases to 3 (Figure 3b) and 4 (Figure 3c). In each case, these regions are separated by about 100 km, so the wider sloping topography regions support more baroclinic jets and Eulerian overturning cells. The distribution of these azimuthal jets is evident in the square root of the mean surface kinetic energy for the case in Figure 3b, as shown in Figure 3d. There is some variability in the azimuthal direction (and in time), but the overall pattern of concentrated momentum separated by regions of weaker flow can be found all around the island. In some regions, a single jet splits into multiple jets, so the quantization described above is only approximate. The width of these jets seems to scale with the baroclinic deformation radius. Calculations with lower/higher values of f result in fewer/more jets over the slope. Similarly, decreasing the offshore stratification produces more, narrower, jets. This is similar to the scaling of multiple jets found by *Condie and Rhines* [1994] for convectively forced flows over a sloping bottom in laboratory experiments.

2.2. Momentum Budgets

[14] The terms in the azimuthal momentum balance have been calculated by rotating the x and y components into the azimuthal (u, positive with shallow water on the left) and radial (v, positive toward shallow water) directions. Because the integration is along a closed contour, the pressure gradient term and the azimuthal advection term integrate to zero.

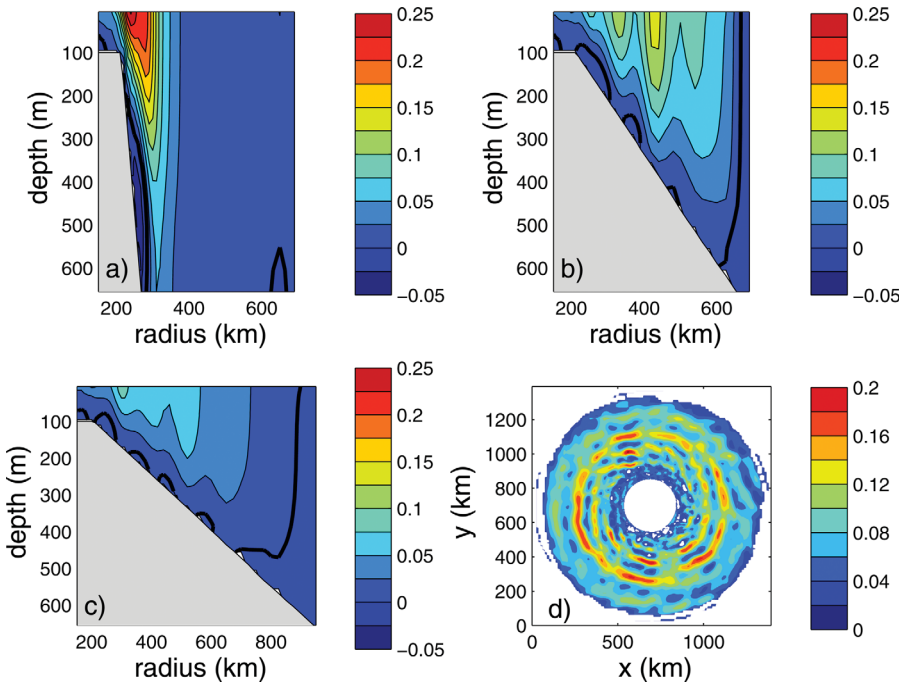

Figure 3. Mean sections of azimuthal velocity for calculations with bottom slopes of (a) 1×10^{-2}; (b) 1.25×10^{-3}; (c) 7.5×10^{-4} (the zero contour is bold); and (d) square root of the mean surface kinetic energy for the case with bottom slope 1.25×10^{-3} (units m s^{-1}, c.i. = 0.02, values less than 0.02 are white).

The model has been integrated long enough that the momentum budget is in statistical steady state. The terms in the momentum equations, averaged over 200 days, integrated around the island, and contoured as a function of depth and radius, are shown in Figure 4 (the quantities are flux divergences of azimuthal momentum). The balance is dominated by three terms: the Coriolis term, bottom drag, and nonlinear horizontal advection. The Coriolis term reflects the

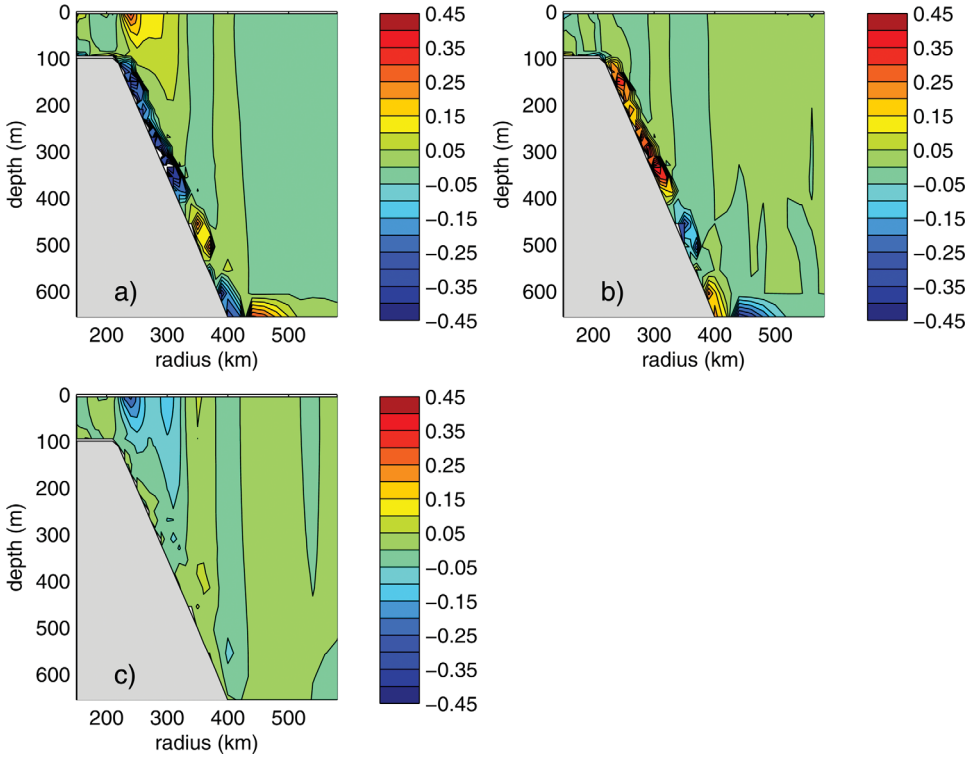

Figure 4. Mean sections of terms in the azimuthal momentum equation. (a) Coriolis term; (b) lateral viscosity and quadratic bottom drag; and (c) advection (units m^2 s^{-2}).

ageostrophic radial transport. The Coriolis force in the bottom boundary layer (Figure 4a) is balanced by the quadratic bottom drag (Figure 4b), consistent with an Ekman layer balance. The Coriolis force associated with the onshore flow above the sloping bottom is balanced by the nonlinear advection term (Figure 4c), primarily the eddy driven radial advection of relative vorticity of the azimuthal velocity, or the Reynolds stress divergence. Note that for a downwelling favorable surface wind stress, as in *Stewart and Thompson* [2012], an onshore flow to balance offshore transport in the bottom boundary layer can be achieved without the nonlinear advection term. Here, the onshore flow causes the Coriolis force to accelerate the azimuthal flow and the eddies decelerate the flow. However, eddies transport this positive azimuthal momentum offshore, where it accelerates the jet over the outer slope and flat bottom, similar to the middepth balance in the Antarctic Circumpolar Current [*Stevens and Ivchenko*, 1997]. This is ultimately damped in the viscous bottom boundary layer.

[15] Kelvin's theorem for a linear, quasigeostrophic circulation shows that the circulation integral around any closed potential vorticity contour requires that the net applied stress be balanced by dissipation [*Pedlosky et al*., 1997]. For a barotropic fluid with no surface stress, or a deep layer isolated from the surface, this requires that the net dissipation around a closed potential vorticity contour be zero. If the contour is along the island boundary, this constraint applies even for nonlinear and primitive equation flows (because of the no normal flow boundary condition). This imposes a strong constraint on the flow, often resulting in recirculations or compensating flows on opposite sides of an island [e.g., *Pedlosky et al*., 1997, 2011; *Spall*, 2000; *Yang*, 2007]. The circulation resulting from cooling over the island shelf drives a flow around the island that is of the same sign all along the topographic contours. This would seem to violate the circulation integral described by the above quasigeostrophic or flat-bottom models. In the present primitive equation model, the dissipation over the sloping bottom is balanced locally by the Coriolis force. This net momentum flux is carried by the ageostrophic velocity in the bottom boundary layer, and thus is not represented in quasigeostrophic theory or for islands with a vertical boundary.

3. Water Mass Transformation

[16] The cooling over the shelf is balanced by a net heat flux across the shelf break. Because there is little mean flow on/off the shelf, and the heat transport is dominated by eddy fluxes, the onshore/offshore transport of water and the water mass transformation are best revealed by the transport streamfunction as a function of offshore distance and temperature (Figure 5). The strongest water mass transformation takes place on the shelf where the surface cooling is active, at radius less than 200 km. The water advected onto the shelf ranges in temperature from about 2.5°C to 5.5°C. The total exchange across the shelf break is 0.60Sv, where $1\text{Sv} = 10^6\ \text{m}^3\text{s}^{-1}$. The source of this water is the offshore restoring region at radius greater than 650 km. This is similar to the deep overturning cell found by *Stewart and Thompson* [2012]. It is interesting that the source waters are drawn onshore from the same density class as is exchanged with the shelf, primarily between 3.5°C and 5°C. These

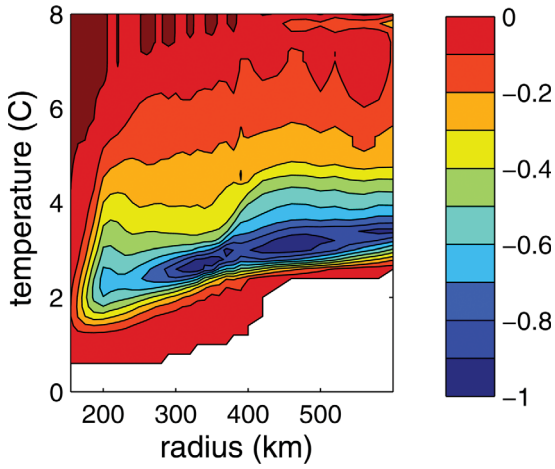

Figure 5. Mean transport streamfunction ($10^6\ \text{m}^3\ \text{s}^{-1}$) as a function of temperature and radius.

waters originate at an offshore depth of approximately 200–500 m. The warmer waters above are largely passive in the heat budget, although they do contribute to the lateral density gradient over the continental slope and thus influence the strength of the jet over the topography.

[17] The dense waters formed over the shelf are returned to the deep ocean between temperatures 1°C and 2.25°C. These densest waters warm steadily as they are moved downslope so that they are between 2.5°C and 3°C when they reach the flat interior (radius greater than 400 km). This warming is offset by cooling of the warm waters as they are carried toward the shelf, particularly near the transition between onshore and offshore flow (2.5°C).

[18] The relative contributions from mean and eddy heat fluxes are complex. The vertically and azimuthally integrated onshore heat flux is shown in Figure 6. The first thing to note is that the total flux is positive in the interior (heat flowing toward the shelf) and nearly constant offshore of the cooling region. This is expected in steady state since there is no heat flux at the surface or bottom away from the shelf. The heat flux rapidly drops to zero over the shelf, with the flux divergence largest near the shelf break. The heat flux over the shelf is dominated by the eddy flux,

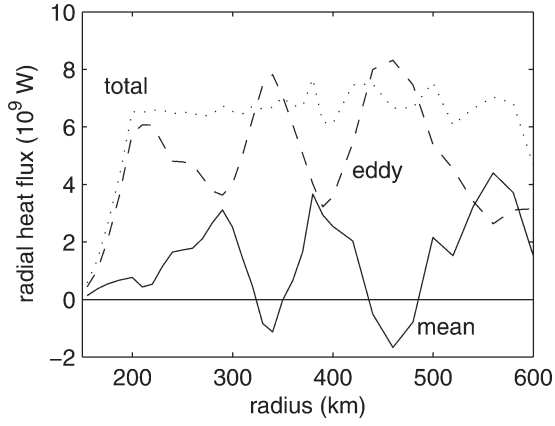

Figure 6. Radial heat flux. Solid line: mean; dashed line: eddy; dotted line: total.

although there is a weak onshore heat flux due to the mean flow. This differs significantly from marginal seas subject to buoyancy loss, where the heat is provided to the basin primarily by mean advection in a cyclonic boundary current [*Spall*, 2010]. However, the eddy flux decreases and the mean flux increases over the sloping bottom such that the mean and eddy contributions are equally important near 250–300 km radius, at the middle of the continental slope. This is where the mean Eulerian flow is onshore throughout the water column and offshore in the bottom boundary layer. This thermally direct cell is sufficiently strong to be significant in the heat budget. Because the total onshore heat flux in this region must be constant, the eddy heat flux has to decrease. Offshore of this, where the bottom velocity changes sign, the mean heat flux drops to less than zero, consistent with the change in sign of the Eulerian overturning circulation. This is compensated by an increase in the eddy heat flux. A similar transfer of heat transport between mean and eddy components takes place as one moves across the thermally direct and indirect cells further offshore.

[19] The regions where the mean heat flux is toward the shelf are also the regions where the Coriolis force is accelerating the azimuthal flow above the bottom boundary layer. This is balanced by a momentum flux divergence in the nonlinear terms (azimuthal momentum is exported by eddies). Conversely, the regions where the mean heat transport is away from the shelf are regions where the eddy momentum flux convergence is driving the azimuthal flow. This is also coincident with the regions of strongest positive eddy heat flux. This is consistent with baroclinic instability and positive heat flux, as summarized by *Vallis* [2006, pp. 487–493]. These multiple regions of momentum flux convergence and divergence emerge spontaneously. For very narrow topography (60 km wide), there are two regions with peak eddy heat flux, one at the shelf break and one over the slope. For the wider sloping regions shown in Figure 3, each region of momentum flux convergence and a thermally indirect overturning cell corresponds with the location of peak eddy heat flux.

3.1. Shelf Water Temperature

[20] Similar patterns of circulation and dense water formation are found over a wide range of parameter space, and so it is of interest to better understand what controls the properties of waters formed over the shelf (e.g., temperature, exchange rate with the open ocean) and how they depend on the parameters that define the island and forcing. The starting point is the heat balance over the shelf. Taking advantage of the finding that the heat transport across the shelf break is dominated by eddy fluxes, the heat budget over the shelf may be written as a balance between the integral of the lateral eddy heat flux and exchange with the atmosphere.

$$\int_0^H \int_P \overline{v'T'}\,\mathrm{d}s\mathrm{d}z = \frac{A\Gamma(T-T_A)}{\rho_0 C_p}, \tag{1}$$

where the overbar denotes a time average, primes indicate perturbations from the time mean, v' is the velocity component directed toward the island, P is the perimeter of the shelf (at the radius of the shelf break), A is the surface area of the shelf, H is the shelf depth, ρ_0 is a representative ocean density, and C_p is the specific heat of seawater. T_A is the spatial average of the atmospheric temperature over the shelf, T is the temperature of water formed on the shelf.

[21] The vertically averaged eddy heat flux may be parameterized as being proportional to the baroclinic velocity in the shelf break jet U and the temperature difference between the water offshore of the shelf, T_1, and the water on the shelf, T [*Visbeck et al.*, 1996; *Spall*, 2004, 2011].

$$\overline{v'T'} = cU(T_1 - T). \tag{2}$$

[22] The problem has been simplified by assuming that the waters over the shelf and the water just offshore of the shelfbreak can be represented by single temperatures T and T_1. This is clearly an oversimplification compared to the model fields in Figure 2, but represents a useful idealization of the bulk characteristics of the model fields that allows for analytic progress to be made. It is assumed that the eddy flux arises from the baroclinic shear across the shelf. The coefficient c in general depends on the bottom slope, but has been found empirically from model and laboratory experiments for a flat bottom, appropriate for the shelf, to be $c = 0.025$ [*Visbeck et al.*, 1996; *Spall*, 2004].

[23] The depth-averaged baroclinic velocity of the rim current is assumed to be in thermal wind balance, so it depends linearly on the density difference across the shelf break jet.

$$U = \frac{gH}{2\rho_0 f_0 L}\alpha(T_1 - T), \tag{3}$$

where g is the gravitational acceleration and α is the thermal expansion coefficient (units $\mathrm{kg\,m^{-3}C^{-1}}$). It has been assumed that U is the vertical average of the baroclinic velocity that arises from a uniform (in depth) horizontal density gradient of $\alpha(T_1 - T)/L$, where L is the width of the shelf and represents the lateral scale over which the temperature changes from its offshore value T_1 to the shelf value T. One could also choose the baroclinic deformation radius for this scale. This smaller scale is more appropriate for wide shelves subject to strong atmospheric forcing, quantified by the nondimensional numbers below, but the overall dependence of the properties of water mass transformation are not overly sensitive to this choice.

[24] Using these conditions, the heat balance may be written as

$$\frac{gcPH^2}{2\rho_0 f_0 L}\alpha(T_1 - T)^2 = \frac{A\Gamma(T - T_A)}{\rho_0 C_p}. \tag{4}$$

[25] Equation (4) is the same equation as arises for thermally forced convection in a marginal sea with a sill [*Spall*, 2011] except two of the parameters is defined differently. Here, L and H are the width and depth of the shelf, whereas in *Spall* [2011], they are the width and depth of the sloping topography that enters the marginal sea from the open ocean. All variables in (4) are known except the temperature of the shelf water, T. Equation (4) can be solved for the nondimensional temperature difference between the shelf and the rim current $\Delta T = (T_1 - T)/T^*$, where the natural temperature scale in the problem is defined by

$T^* = T_1 - T_A$, the difference between the offshore temperature and the temperature of the atmosphere over the shelf. Following *Spall* [2011], the solution for the temperature anomaly of the shelf water is

$$\Delta T = \mu/\epsilon\left[(1+2\epsilon/\mu)^{1/2} - 1\right]. \quad (5)$$

[26] There are two nondimensional numbers that define the solution. The ratio of the heat fluxed onto the shelf by eddies compared to that advected around the island (relative to T) is $\epsilon = cP/L$ [*Spall*, 2004]. The value of ϵ is very small for stable currents and large for unstable currents.

[27] The nondimensional parameter μ is defined as

$$\mu = \frac{A\Gamma f_0}{\alpha g C_p H^2 T^*}. \quad (6)$$

[28] As discussed by *Spall* [2011], μ/ϵ is a measure of the relative influence of cooling by the atmosphere compared to lateral eddy heat fluxes from the rim current in the shelf heat budget. For $\mu/\epsilon \ll 1$, lateral eddy heat flux from offshore is very strong and leads to a relatively warm shelf (compared to the atmospheric temperature), i.e., $T \approx T_1$. For $\mu/\epsilon \gg 1$, the shelf break jet is relatively stable and the atmosphere is able to strongly cool the shelf so that $T \approx T_A$.

[29] An approximate solution can be derived [*Spall*, 2011] as

$$\Delta T = \frac{2\mu/\epsilon}{1+2\mu/\epsilon}. \quad (7)$$

[30] This is obtained by assuming for the purposes of the eddy flux parameterization that the shelf water temperature is T_A, which will generally overestimate the eddy heat flux. This is a good approximation for $\mu/\epsilon \geq O(1)$ but overestimates the temperature anomaly of the shelf water for $\mu/\epsilon \ll 1$. This approximate solution is useful for the interpretation of the diapycnal mass flux in the following section.

[31] A series of 17 numerical model calculations have been carried out in which the parameters that define the shelf region and forcing have been varied (summarized in Table 1). The offshore temperature T_1 is taken to be 5.8°C, the depth average of the temperature in the offshore restoring region. The dimensional temperature predicted by (4) generally compares well with that diagnosed from the model calculations (Figure 7a). The solid square symbol is the calculation discussed above (run 1 in Table 1), and the asterisk is a similar calculation with canyons and ridges (discussed in the following section). The change in temperature across the shelf ranges from less than 1°C to approximately 5.8°C. There is a dependence of the shelf water temperature on the offshore slope, which is not considered in the theory. The symbols all at the same theoretical value as the solid square differ only in their bottom slope offshore of the shelf break. A bottom slope of 1.25×10^{-3} produces warmer shelf water while a bottom slope of 0.01 results in cooler shelf water compared to the standard case with bottom slope of 0.003 (runs 2 and 3). The reason for this dependence is not clear but may be a result of c being dependent on the offshore slope.

[32] Table 1 documents how the temperature of the waters on the shelf varies with the model parameters, but it is more revealing to plot the nondimensional temperature anomaly of the shelf water ΔT versus the nondimensional number μ/ϵ. Small values of μ/ϵ produce small values of ΔT, or relatively warm product waters. This is because the shelf break front is relatively efficient at transporting water across the shelf break. For large values of μ/ϵ, eddy fluxes are not very effective at transporting heat and the product water on the shelf is very cold. The trend predicted by the theory is reproduced well by the model. The approximate analytic solution given by (7) is indicated by the dashed line. As mentioned above, it compares well with the full theory for $\mu/\epsilon \geq O(1)$, but generally underpredicts the temperature anomaly of the shelf water for $\mu/\epsilon \ll O(1)$.

Table 1. Summary of Model Runs With Key Parameters[a]

Run	H	R_c	F_0	L	s	α	Γ	μ/ϵ	T_1-T	Ψ^*
1	100	200	10^{-4}	75	0.003	0.2	47.5	1.4	4.6	0.60
2	100	200	10^{-4}	75	0.01	0.2	47.5	1.4	4.8	0.53
3	100	200	10^{-4}	75	0.00125	0.2	47.5	1.4	3.8	0.84
4	200	200	10^{-4}	75	0.003	0.2	47.5	0.34	3.7	0.97
5	50	200	10^{-4}	75	0.003	0.2	47.5	5.5	5.5	0.31
6	100	300	10^{-4}	150	0.003	0.2	47.5	7.0	5.0	0.38
7	100	200	1.5×10^{-4}	75	0.003	0.2	47.5	2.0	5.1	0.42
8	100	200	0.5×10^{-4}	75	0.003	0.2	47.5	0.68	4.1	0.92
9	200	200	10^{-4}	75	0.003	0.2	15.8	0.11	2.8	0.55
10	200	200	10^{-4}	75	0.003	0.2	7.9	0.06	1.86	0.42
11	250	200	0.5×10^{-4}	75	0.003	0.2	4.0	0.01	0.5	0.45
12	50	300	1.5×10^{-4}	150	0.003	0.2	47.5	42	5.8	0.25
13	250	300	0.5×10^{-4}	150	0.003	0.2	4.0	0.04	1.7	0.74
14	100	200	10^{-4}	75	0.003	0.1	47.5	2.7	5.1	0.33
15	250	300	0.3×10^{-4}	150	0.003	0.2	4.0	0.02	1.7	0.97
16	250	300	0.3×10^{-4}	150	0.003	0.2	8.0	0.04	1.9	1.4
17	250	200	0.3×10^{-4}	75	0.003	0.4	4.0	0.005	0.2	0.66

[a]Sill depth H (m); cooling radius R_c (km); Coriolis parameter (10^{-4} s^{-1}); shelf width L (km); topographic slope (s); thermal expansion coefficient (kg m^{-3} C^{-1}; relaxation constant Γ (W m^{-2} C^{-1}); μ/ϵ. The model diagnosed quantities: temperature anomaly of the shelf water mass (T_1-T, °C); maximum diapycnal streamfunction at shelf edge (10^6 m^{3}S^{-1}).

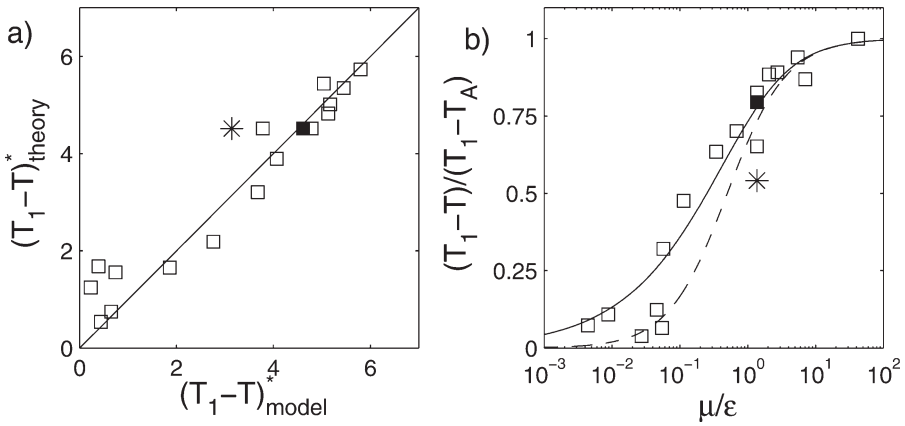

Figure 7. Average temperature anomaly of water on the shelf from theory and a series of model calculations: (a) dimensional (C) and (b) nondimensional.

3.2. Diapycnal Mass Flux

[33] Once the average temperature of the waters on the shelf is known, an expression for the diapycnal mass flux across the shelfbreak can be derived as that required to balance the heat loss to the atmosphere over the shelf. This is equivalent to the rate of dense water formation, and so is a quantity of general interest for understanding the ocean's thermohaline circulation and how it might vary in a changing climate. This balance can be written as

$$\Psi^*(T_1 - T) = \frac{2A\Gamma}{\rho_0 C_p}(T - T_A), \tag{8}$$

where Ψ^* is the maximum absolute (dimensional) diapycnal transport streamfunction at the shelfbreak. It has been assumed in this derivation that the average temperature of the water transported onto the shelf is $0.5(T_1 + T)$. This is motivated by the transport streamfunction in temperature coordinates in Figure 5, where it was shown that water is carried onto the shelf above the bottom boundary layer. If it is assumed that all the water transported onto the shelf is of temperature T_1, the right-hand side of (8) is reduced by a factor of 2, but is otherwise unchanged. The assumption that all the shelf water is of temperature T will provide a low estimate of the diapycnal transformation because, near the shelf break, some water will be warmer because of the tilting of the isotherms over the shelf (Figure 2).

[34] The diapycnal streamfunction can be solved for as:

$$\Psi^* = \frac{2A\Gamma}{\rho_0 C_p}(1/\Delta T - 1), \tag{9}$$

where the nondimensional ΔT is given by (5). If $A\Gamma/\rho_0 C_p$ remains nonzero, it is evident that as $\Delta T \to 0$, Ψ^* will become large. This is because the heat transport onto the shelf is proportional to the product of the transport Ψ^* and $T_1 - T$. As the shelf warms, the heat loss to the atmosphere increases but achieving a net heat flux onto the shelf requires an ever-increasing mass transport because $T_1 - T \to 0$.

[35] It is useful to use the approximate solution for ΔT, (7), which then simplifies the diapycnal streamfunction to be

$$\Psi^* = \epsilon/\mu\left[\frac{A\Gamma}{\rho_0 C_p}\right] = \epsilon\left[\frac{\alpha g H^2 T^*}{\rho_0 f_0}\right]. \tag{10}$$

[36] There are two natural mass transport scales in the problem. The quantity $A\Gamma/\rho_0 C_p$ has the units of mass transport and represents the strength of atmospheric forcing. The quantity in the second brackets in (10) is the geostrophic mass transport that results from a horizontal temperature change of T^* over a depth of H. Note that in this limit of large μ/ϵ, the water mass transformation is independent of the atmospheric restoring constant Γ. Consider an increase in Γ for $\mu/\epsilon \gg 1$. This will cause a nearly linear decrease in the temperature anomaly of the shelf water. However, the heat loss to the atmosphere will linearly increase because of the increase in Γ. As a result, the diapycnal streamfunction becomes independent of the change in Γ.

[37] The maximum transport streamfunction in temperature coordinates at the radius of the shelf break was diagnosed for each of the model calculations (as in Figure 5) and is plotted (scaled by $\frac{A\Gamma}{\rho_0 C_p}$) against μ/ϵ in Figure 8. The solid square symbol is the standard case discussed above. The streamfunction is small for large μ/ϵ and increases

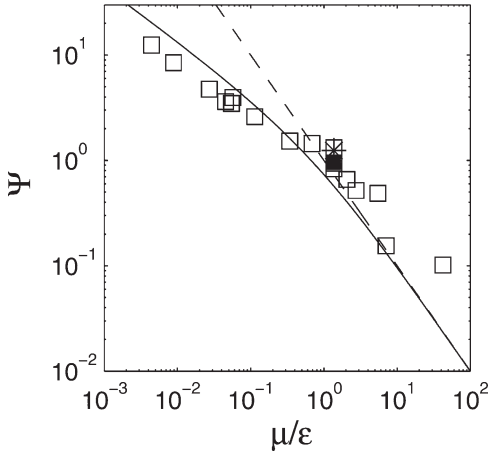

Figure 8. Nondimensional diapycnal transport across the shelf break from theory and a series of model calculations.

rapidly for small μ/ϵ, as predicted by the full theory (10), solid line. Although there is some scatter, the general dependence of the diapycnal mass flux on μ/ϵ is predicted reasonably well. There is some dependence on the bottom slope, as expected from the change is shelf temperature, but this is small compared to the changes induced by the other model parameters. Small μ/ϵ corresponds to strong lateral eddy fluxes, which emphasizes the role in eddies in supporting the diapycnal mass flux and water mass transformation. In general, smaller f_0, deeper shelves, and larger air-sea temperature differences lead to stronger diapycnal mass fluxes.

4. Canyons and Ridges

[38] The topography in the previous sections was uniform in the azimuthal direction. While useful as a starting point, one would also like to understand how topography that varies around the island alters the previous balances. Momentum balances in a model of the ACC indicate that pressure changes across topographic ridges are of leading order importance [*Stevens and Ivchenko*, 1997]. A calculation has been carried out with a series of ridges and canyons around an island, as shown in Figure 9. The maximum bottom slope is .0045 and minimum bottom slope is .0015, this gives a maximum change in bottom depth from crest to trough of 400 m at a radius of 358 km.

[39] The temperature, azimuthal velocity, radial velocity, and vertical velocity averaged as a function of radius and depth are shown in Figure 10. The topography shown is the deepest topography found at each radius. The temperature and azimuthal velocity are similar to what was found for the case with no ridges or canyons. Dense water formed over the shelf penetrates downslope, resulting in sloping isopycnals and an azimuthal jet with reversed flow near the bottom. The radial velocity is much more complex, however, with a region of strong upslope flow over the midslope. This is likely related to a phase shift in the direction of wave propagation relative to the topography [*Brink*, 2010]. There is also reversing upslope and downslope flow over the outer topography and flat bottom. Similar to the previous cases, an Ekman layer with downslope flow and onshore flow above is found very near the top of the sloping region. The vertical velocity takes an alternating upwelling/downwelling pattern centered within the canyons.

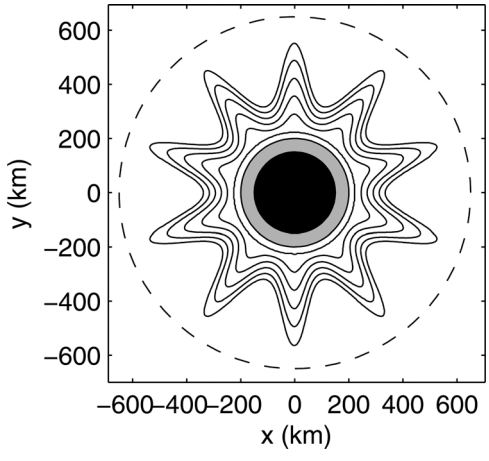

Figure 9. Bottom topography for calculation with canyons and ridges. Cooling is over the shelf (light gray area) and full depth restoring is at radius greater than 650 km (dashed line).

[40] A simpler picture emerges if the averaging is done along topographic contours so that the azimuthal velocity is parallel to, and the radial velocity is perpendicular to, the local topographic contours (Figure 11). (A very weak linear topographic slope has been added to the shelf and deep ocean so that depth contours are available for the coordinate transformation.) The temperature, azimuthal velocity, and radial velocity are now quite similar to that found for the calculations without ridges and canyons. There is a narrow region of strong downslope flow along the sloping bottom with weaker onshore flow throughout the water column above. The vertical velocity is now dominated by upwelling over the outer slope and downwelling over the upper slope. Even though the average width of the sloping bottom is wider than that in the central case above, multiple jets do not develop. It is likely that this is controlled by the narrowest region of topography because all transport has to pass through this constriction when encircling the island.

[41] Variable topography introduces the possibility that the pressure gradient term might become important in the azimuthal momentum balance because the pressure can vary from one side of the topography to the other [*Stevens and Ivchenko*, 1997]. The terms in the azimuthal momentum equation are plotted as a function of radius and depth in Figure 12. Near the surface, the balance is between the Coriolis term and the nonlinear advection term, as found previously, except that there is now a pattern of alternating positive and negative bands over the topography, as found for the radial velocity in Figure 10. The dissipation term is much smaller than for the case with no ridges. Above the sill crests the pressure gradient term is small, as expected because it is periodic. However, the pressure gradient term is large in the depth range between the crests and troughs, where it is balanced by the Coriolis term. The pattern reflects regions of positive and negative values, which are interpreted as regions of geostrophically balanced upslope (positive Coriolis) and downslope (negative Coriolis) flows.

[42] A different picture of the momentum balance emerges if the azimuthal direction is taken as that which is locally parallel to, and the radial direction is that perpendicular to, the topographic contours. In that case, the flow breaks down into the same two regimes as found for the case with no ridges and canyons. Above the bottom boundary layer, the balance is largely between the Coriolis term and the nonlinear advection term (Figure 13). Very near the bottom, the balance is between the Coriolis term and dissipation (the bottom Ekman layer). The pressure gradient term is essentially zero everywhere (there is a small residual as a result of rotating the terms in the momentum equation into topographic coordinates, not shown). A similar result was found by *Brink* [2010] for barotropic flow over variable bottom topography forced by oscillating winds. Thus, the basic dynamical regimes are identical to that found for azimuthally uniform topography. The pressure term may, of course, become important for configurations with regions of blocked topographic contours that do not encircle the island, such as might be expected for deep ocean ridges that connect the island to a continent.

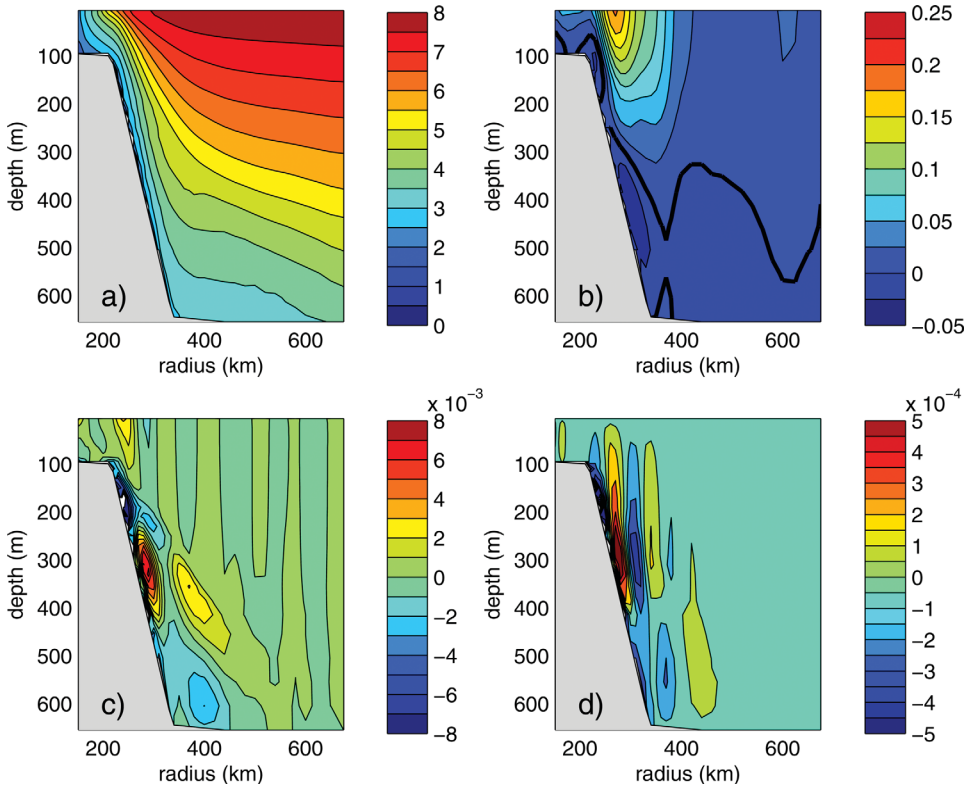

Figure 10. Mean sections in depth/radius coordinates of (a) temperature (°C); (b) azimuthal velocity (m s^{-1}); (c) radial velocity (m s^{-1}); and (d) vertical velocity (m s^{-1}).

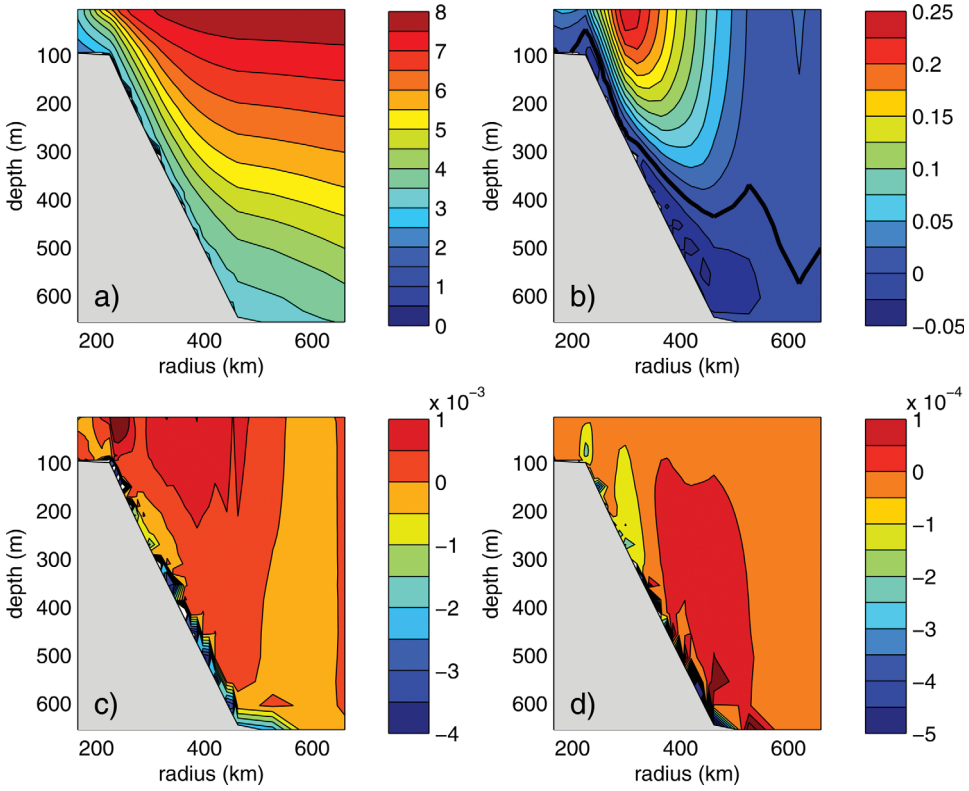

Figure 11. Mean sections rotated into topographic coordinates of (a) temperature (°C); (b) azimuthal velocity (m s^{-1}); (c) radial velocity (m s^{-1}); and (d) vertical velocity (ms^{-1}).

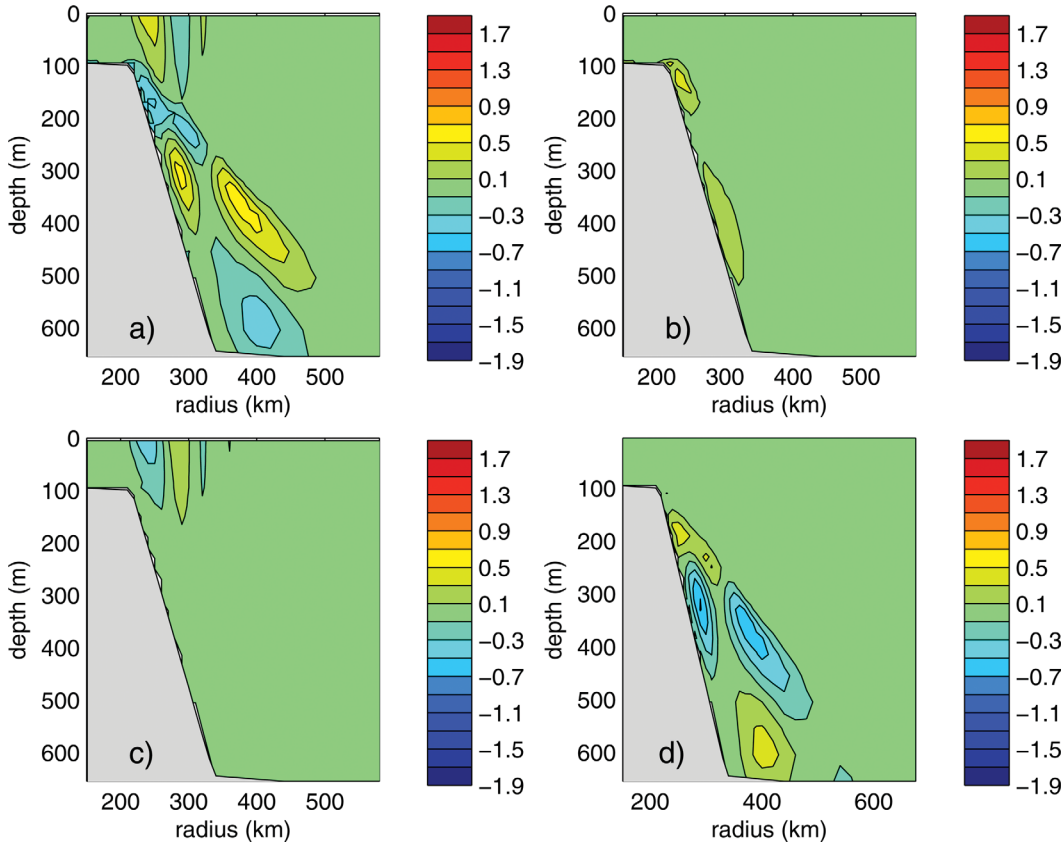

Figure 12. Mean sections of terms in the azimuthal momentum equation averaged as a function of radius and depth for the case with ridges and canyons. (a) Coriolis term; (b) lateral viscosity and quadratic bottom drag; (c) advection; and (d) azimuthal pressure gradient (units $m^2\ s^{-2}$).

[43] The diapycnal transport streamfunction for this case is shown in Figure 14. The streamfunction is first calculated along constant depth contours, as were the terms in the momentum balance, then plotted as a function of the average radius of each depth contour. The general pattern is very similar to the standard case with uniform topography. There is less diapycnal mixing over the sloping bottom, perhaps related to the lack of multiple jets. The water transported onto the shelf is also warmer than the uniform topography previous case. The shelf water temperature and diapycnal transport are indicated in Figures 7 and 8 by the asterisk. The shelf water is warmer for the case with ridges and canyons and, as a result, the diapycnal transformation is larger than the standard case with uniform topography (0.79 Sv compared to 0.60 Sv). The larger transformation is consistent with the warmer shelf water found with ridges and canyons. The case with ridges and canyons has an average bottom slope of 0.0022, approximately 27% less than the standard case with uniform topography and slope 0.003. Thus, the increase in transformation is at least partly consistent with the decrease in bottom slope, but that does not appear to explain all the increase.

5. Summary

[44] The general issue of dense water formation around islands has been considered using idealized numerical models and simple theoretical constraints. It was shown that dense water formed over an island shelf is exported to the slope region largely by lateral eddy fluxes. This is consistent with previous findings for dense water formation over a shelf [*Gawarkiewicz and Chapman*, 1995; *Jiang and Garwood*, 1996; *Kikuchi and Wakatsuchi*, 1999; *Pringle*, 2001]. The present focus is more on the momentum balances over the slope and the diapycnal mass flux between the deep ocean and the shelf. Once over the continental slope, the heat transport is carried by a combination of mean Eulerian overturning cells and lateral eddy fluxes. The overturning cells are coincident with rectified azimuthal baroclinic jets, which emerge naturally from the turbulent flow. They scale with the baroclinic deformation radius and are dynamically similar to the midlatitude atmospheric zonal flows and the Hadley and Ferrel cells. The Eulerian downwelling of dense water is concentrated in the bottom Ekman layer, but it is dynamically connected to the upper ocean eddy momentum flux divergence due to the Reynolds stress term. This is fundamentally different from the momentum balance in marginal seas subject to buoyancy forcing, in which the downwelling is balanced by the pressure gradient along the boundary. It was also shown that the basic momentum balances are not altered by the presence of ridges and canyons in the topography. The apparent importance of form stress supported by pressure gradients across the topography is eliminated if the balance

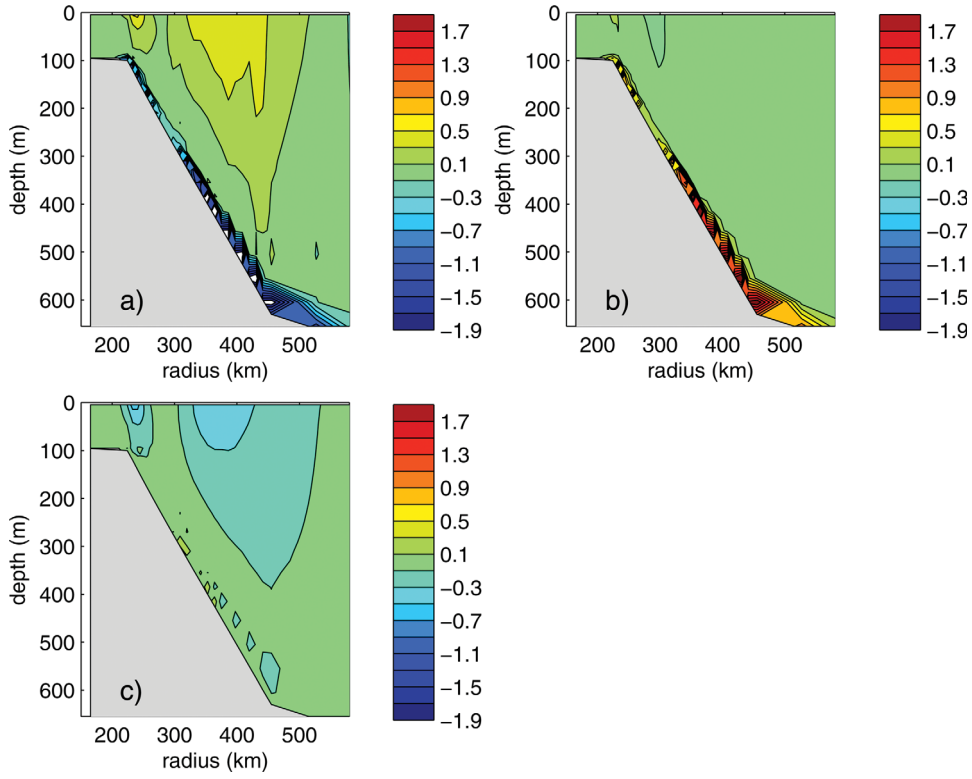

Figure 13. Mean sections of terms in the momentum equation rotated along topographic contours for the case with ridges and canyons. (a) Coriolis term; (b) lateral viscosity and quadratic bottom drag; and (c) advection (units $m^2\ s^{-2}$).

is viewed in a coordinate frame rotated in the direction of the topography.

[45] The properties of the dense water formed over an island shelf can be estimated using a heat budget and a parameterization of baroclinic instability. The resulting estimate for the temperature of the shelf water is functionally the same as a recent result for convective water masses formed in a marginal sea by *Spall* [2011], although the parameters are defined slightly differently. The main result, however, is that the density anomaly of the shelf waters depends on a nondimensional number μ/ϵ, which represents

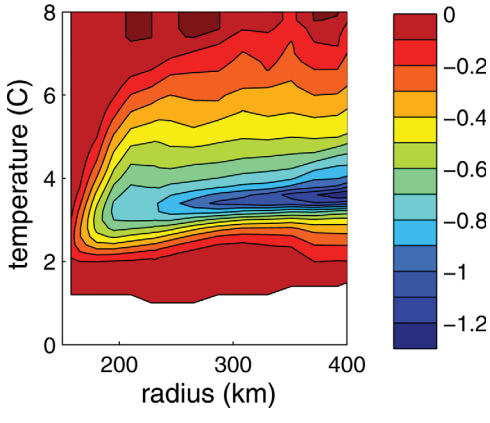

Figure 14. Mean transport streamfunction ($10^6\ m^3\ s^{-1}$) as a function of temperature and radius for the calculation with ridges and canyons.

the competition between the atmosphere cooling the shelf and lateral eddy fluxes warming the shelf and is derived from the model topography, Coriolis parameter, and properties of atmospheric forcing. The diapycnal transport streamfunction, or water mass formation rate, can also be estimated from the theory and depends on μ/ϵ. The temperature and water mass transformation rate diagnosed from a series of numerical model calculations compares reasonably well with that predicted by the theory, although there is a weak dependence on the offshore topographic slope that is not considered in the theory. Ridges and canyons also influence the quantitative values of the shelf waters and transformation, but the overall picture is consistent with that predicted by the simple theory that assumes symmetric topography.

[46] The problems considered here have been simplified in many ways that, while key to obtaining a single theoretical framework with which to interpret the results, distances these results from direct application to any one particular region. Important aspects neglected here include spatially variable forcing; large-scale, remotely forced, circulations; wind-forcing; time-dependent forcing. The present results are far from comprehensive, but do provide a basic framework from which to consider these additional forcing effects and to distinguish the lowest order aspects of water mass transformation around an island from the more often studied problem of open ocean deep convection and water mass transformation in marginal seas. Many aspects of these results are also expected to be relevant for buoyancy forced circulations in enclosed basins and around submarine topographic features with closed f/h contours, both of

which have periodic boundary conditions along the topography.

Appendix A: Numerical Model Configuration

[47] The numerical model used in this study is the MIT general circulation model [*Marshall et al.*, 1997], which solves the hydrostatic primitive equations on a uniform Cartesian, staggered C-grid with level vertical coordinates.

[48] The surface heat flux in the model (Q^*) is calculated by restoring the upper level temperature T toward a prescribed atmospheric temperature T_A as $Q^* = (T - T_A)\Gamma$, where Γ is a restoring constant with units W m^{-2} C^{-1}. For all calculations here, $T_A = 0$. The temperature outside a radius of 650 km is also restored toward a profile with uniform vertical stratification of $N^2 = (g/\rho_0)\partial\rho/\partial z = 2 \times 10^{-6}\mathrm{s}^{-2}$ and an upper level temperature of 8°C with a time scale of 10 days.

[49] The model incorporates second-order vertical viscosity and diffusivity with coefficients $10^{-5}\mathrm{m}^2\mathrm{s}^{-1}$. The vertical diffusion is increased to 1000 $\mathrm{m}^2\mathrm{s}^{-1}$ for statically unstable conditions in order to represent vertical convection. Horizontal viscosity is parameterized as a second-order operator with the coefficient A_h determined by a Smagorinsky closure as $A_h = (\nu_s/\pi)^2\Delta^2\left[\left(u_x - v_y\right)^2 + \left(u_y + v_x\right)^2\right]^{1/2}$, where $\nu_s = 2.5$ is a nondimensional coefficient, Δ is the grid spacing, and u and v are the horizontal velocities (subscripts indicate partial differentiation). Temperature is advected with a third-order direct space time flux limiting scheme (MITgcm tracer advection option 33, http://mitgcm.org). There is no explicit horizontal diffusion of temperature. Density is linearly related to temperature as $\rho = \rho_0 - \alpha T$, where α is the thermal expansion coefficient with units kg m^{-3}C^{-1}.

[50] **Acknowledgments.** This study was supported by the National Science Foundation under grants OCE-0850416, OCE-0959381, and OCE-0859381. Comments and suggestions from anonymous reviewers helped to clarify the presentation. Any opinions, findings, and conclusions or recommendations expressed in this material are those of the author and do not necessarily reflect the views of the National Science Foundation.

References

Blumsack, S. L., and P. J. Gierasch (1972), Mars: The effects of topography on baroclinic instability,. *J. Atmos. Sci.*, *29*, 1081–1089.

Brink, K. H. (2010), Topographic rectification in a forced, dissipative barotropic ocean, *J. Mar. Res.*, *68*, 337–368.

Chapman, D. C., and G. Gawarkiewicz (1997), Shallow convection and buoyancy equilibration in an idealized coastal Polynya, *J. Phys. Oceanogr.*, *27*, 555–566.

Condie, S. A., and P. B. Rhines (1994), Topographic Hadley cells, *J. Fluid Mech.*, *280*, 349–368.

Danielson, S., K. Aagaard, T. Weingartner, S. Martin, P. Winsor, G. Gawarkiewicz, and D. Quadfasel (2006), The St. Lawrence polynya and the Bering shelf circulation: New observations and a model comparison, *J. Geophys. Res.*, *111*, C09023, doi:10.1029/2005JC003268.

Foldvik, A., T. Gammelsrod, S. Osterhus, E. Fahrbach, G. Rohardt, M. Schroder, K. Nicholls, L. Padman, and R. Woodgate (2004), Ice shelf water overflow and bottom water formation in the southern Weddell Sea, *J. Geophys. Res.*, *109*, C02015, doi:10.1029/2003JC002008.

Gawarkiewicz, G., and D. C. Chapman (1995), A numerical study of dense water formation and transport on a shallow, sloping continental shelf, *J. Geophys. Res.*, *100*, 4489–4507.

Isachsen, P. E., and O. A. Nost (2012), The air-sea transformation and residual overturning circulation within the Nordic Seas, *J. Mar. Res.*, *70*, 31–68.

Jiang, L., and R. W. Garwood (1996), Three-dimensional simulation of outflows on continental slopes, *J. Phys. Oceanogr.*, *26*, 1214–1233.

Kikuchi, T., and M. Wakatsuchi (1999), A numerical investigation of the transport process of dense shelf water formation from a continental shelf to a slope, *J. Geophys. Res.*, *104*, 1197–1210.

Marshall, J. C., and F. Schott (1999), Open-ocean convection: Observations, theory, and models, *Rev. Geophys.*, *37*, 1–64.

Marshall, J., C. Hill, L. Perelman, and A. Adcroft (1997), Hydrostatic, quasi-hydrostatic, and non-hydrostatic ocean modeling, *J. Geophys. Res.*, *102*, 5733–5752.

Pedlosky, J., L. J. Pratt, M. A. Spall, and K. Helfrich (1997), Circulation around islands and ridges, *J. Mar. Res.*, *55*, 1199–1251.

Pedlosky, J., R. Iacono, E. Napolitano, and M. A. Spall (2011), The two-layer skirted island, *J. Mar. Res.*, *69*, 347–382.

Pickart, R. S., L. J. Pratt, D. J. Torres, T. E. Whitledge, A. Y. Proshutinsky, K. Aagaard, T. A. Agnewd, G. W. K. Moore, and H. J. Dail (2010), Evolution and dynamics of the flow through Herald Canyon in the western Chukchi Sea, *Deep–Sea Res. II*, *57*, 5–26.

Pringle, J. M. (2001), Cross-shelf eddy heat transport in a wind-free coastal ocean undergoing winter time cooling, *J. Geophys. Res.*, *106*, 2589–2604.

Spall, M. A. (2000), Buoyancy-forced circulations around islands and ridges, *J. Mar. Res.*, *58*, 957–982.

Spall, M. A. (2004), Boundary currents and water mass transformation in marginal seas, *J. Phys. Oceanogr.*, *34*, 1197–1213.

Spall, M. A. (2010), Dynamics of downwelling in an eddy-resolving convective basin, *J. Phys. Oceanogr.*, *40*, 2341–2347.

Spall, M. A. (2011), On the role of eddies and surface forcing in the heat transport and overturning circulation in marginal sea, *J. Clim.*, *24*, 4844–4858.

Spall, M. A. (2012), Influences of precipitation on water mass transformation and deep convection, *J. Phys. Oceanogr.*, *42*, 1684–1700.

Stevens, D. P., and V. Ivchenko (1997), The zonal momentum balance in an eddy-resolving general-circulation model of the Southern Ocean, *Q. J. R. Meteorol. Soc.*, *123*, 929–951.

Stewart, A. L., and A. F. Thompson (2012), Sensitivity of the ocean's deep overturning circulation to easterly Antarctic winds, *Geophys. Res. Lett.*, *39*, L18604, doi:10.1029/2012GL053099.

Straneo, F. (2006), Heat and freshwater transport through the central Labrador Sea, *J. Phys. Oceanogr.*, *36*, 606–628.

Vallis, G. (2006), *Atmospheric and Oceanic Fluid Dynamics*, Cambridge Univ. Press, New York.

Visbeck, M., J. Marshall, and H. Jones (1996), Dynamics of isolated convective regions in the ocean, *J. Phys. Oceanogr.*, *26*, 1721–1734.

Yang, J. (2007), An oceanic current against the wind: How does Taiwan island steer warm water into the east China sea?, *J. Phys. Oceanogr.*, *37*, 2563–2569.